Chem Biol Drug Des 2007; **69:** 99–110

Research Article

doi: 10.1111/j.1747-0285.2007.00484.x

Engineering Metal Complexes of Chiral Pentaazacrowns as Privileged Reverse-turn Scaffolds

Ye Che[1,*], Bernard R. Brooks[1], Dennis P. Riley[2], Andrea J. H. Reaka[3] and Garland R. Marshall[3]

[1]Laboratory of Computational Biology, National Heart, Lung and Blood Institute, National Institutes of Health, Bethesda, MD 20892 USA
[2]Kereos, Inc., 4041 Forest Park Ave, St Louis, MO 63108, USA
[3]Center for Computational Biology and Department of Biochemistry and Molecular Biophysics, Washington University, St Louis, MO 63110, USA
**Corresponding author: Ye Che, chey@nhlbi.nih.gov*
Present address: Andrea J. H. Reaka, SIUE School of Pharmacy, Edwardsville, IL 62026, USA.

Reverse turns are common structural motifs and recognition sites in protein/protein interactions. The design of peptidomimetics is often based on replacing the amide backbone of peptides by a non-peptidic scaffold while retaining the biologic mode of action. This study evaluates the potential of metal complexes of chiral pentaazacrowns conceptually derived by reduction of cyclic pentapeptides as reverse-turn mimetics. The possible conformations of metal complexes of chiral pentaazacrown scaffolds have been probed by analysis of 28 crystal structures complexed with six different metals (Mn, Fe, Co, Ni, Cu, and Zn). The solvated structures as well as the impact of complexation with different metals/oxidation states have been examined with density functional theory (DFT) calculation as explicitly represented by interactions with a single water molecule. The results suggest that most reverse-turn motifs seen in proteins could be mimicked effectively with a subset of metal complexes of chiral pentaazacrown scaffolds with an RMSD of approximately 0.3 Å. Due to the relatively fixed orientation of the pendant chiral side groups in these metal complexes, one can potentially elicit information about the receptor-bound conformation of the parent peptide from their binding affinities. The presence of 20 H-atoms on the pentaazacrown ring that could be functionalized as well as the conformational perturbations available from complexation with different metals offer a desirable diversity to probe receptors for reverse-turn recognition.

Key words: density functional theory, pentaazacrown, peptidomimetics, principal component analysis, privileged structure, protein–protein interaction, reverse turn, template design, transition metal

Received 1 February 2007, accepted for publication 15 February 2007

Reverse turns are common structural motifs and recognition sites in protein/protein interactions (1). Receptor recognition, substrate specificity, and catalytic function generally reside in these loop regions that often connect residues of adjacent α-helices and β-strands contributing to the structural stability of proteins. Examples of turns as recognition motifs can be found in many crystal structures of protein complexes (2–4). Unfortunately, structural information on therapeutic targets is not available for many systems utilizing reverse-turn recognition, such as G-protein-coupled receptors, and indirect approaches are necessary to deduce the sequence location and type of reverse-turn motif. Thus, development of compounds designed to mimic these secondary structural features of reverse turns is an important approach for elucidating the receptor-bound conformation of a biologically active peptide, and potentially, modulate peptide–receptor interactions.

Numerous strategies have been developed to stabilize the reverse-turn conformation in a peptide chain, or to mimic the orientation of side chains of reverse turns with relatively rigid templates [For recent reviews, see Marshall (5), Che (6), Che *et al.* (7), and references therein]. One common approach is to introduce a covalent linkage between residues i and $i + 3$, such as head-to-tail cyclization, while retaining the reverse-turn conformation. Many natural peptides with different kinds of biologic activities, such as hormones, antibiotics, ion-transport regulators, and toxins, are cyclic peptides. They have been reported to bind multiple, unrelated classes of receptors with high affinity. Cyclic peptides are thus considered to be 'privileged structures' capable of providing useful ligands for more than one receptor due to their high content of reverse-turn motifs. For example, Kessler and co-workers (8,9) advocated the use of cyclic pentapeptides (CPPs) as conformationally constrained scaffolds for probing receptor recognition, where a recognition motif (such as RGD) was systematically shifted around cyclic peptide backbone to spatially sample various conformations. However, earlier theoretical and experimental studies have demonstrated a considerable degree of conformational averaging in NMR studies of CPPs advocated as receptor probes (10). This has stimulated Marshall and co-workers (11,12) to propose the use of metal complexes

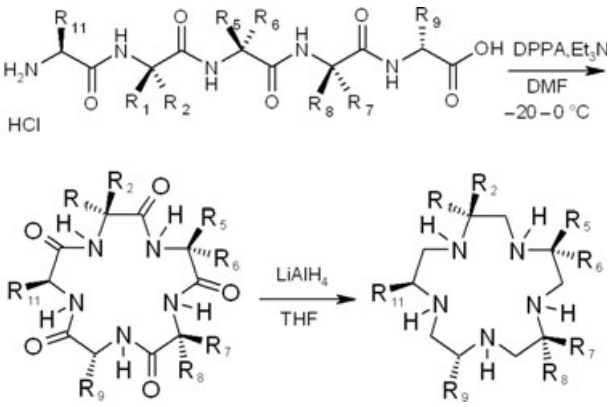

Figure 1: Synthesis of a cyclic pentapeptides followed by reduction of the amide bonds to secondary amines (a logical, but not necessarily optimal, synthetic route) to generate a chiral pentaazacrown.

of chiral azacrowns (MACs) derived from amino acid synthons as a strategy for controlling the conformation and fixing chiral side chains in orientations comparable with those of β-turns. Reduction of the amide bonds to secondary amines of a CPP precursor leads to a flexible chiral pentaazacrown, and the flexibility can be limited by complexation with a metal to fix the side chain orientations to a manageable set (Figure 1) (13). Proof of concept of MACs providing a novel approach to peptidomimetics came from two examples, where the receptor-bound conformations had been previously determined by X-ray crystallography of peptide–receptor complexes (14). One MAC was designed to mimic the proposed receptor-bound conformation of the RGD motif of the cyclic pentapeptide, c[RGDfMeV], complexed with the $\alpha_V\beta_3$ integrin receptor (15). And the other MAC was designed to mimic the α-amylase-bound conformation of a WRY β-turn motif from tendamistat (16,17). In comparison with linear peptides or CPPs, MACs are more stable to peptidases, often more bioavailable, and possess entropic advantages in molecular recognition and binding.

The metal center is buried in the middle of a MAC complex, acting like glue to keep the pharmacophore groups oriented together in their desired directions. One must design a complex which affords the proper geometrical orientations, but it is also essential that the metal be bound tightly so that no redox-active metals are allowed to dissociate from the complex *in vivo* to complicate bioassays with potentially toxic side-effects. Previously, Riley and co-workers (18–25) have demonstrated that MACs possessed catalytic superoxide dismutase (SOD) activity in a wide range of MAC analogs when complexed with manganese. These metal complexes showed reasonable thermodynamic stabilities and excellent kinetic stability with the metal complexes completely intact under physiologic conditions and no metal dissociation for many hours even in the presence of EDTA. Clinical candidates for a variety of inflammation conditions as well as ischemia/reperfusion injury, refractory hypotension, and HIV-1 infection emerged from this class of metal complexes (21,26–28). The fact that one MAC, M40403, has successfully completed Phase I and II clinical trials has demonstrated that this class of metal complexes is relatively safe and possesses suitable pharmacokinetic properties ($\log P$) for use as pharmacologic probes and potential therapeutic agents.

From our point of view, MACs provide an exceptional platform to tailor molecular diversity because they possess both the required limited conformational flexibility of their macrocyclic ring and a great diversity of rigidified spatial combinations of side chains when complexed to different metals. The presence of 10 potentially functionalized and stereochemically controlled centers on the periphery of the macrocycle offers 20 H-atoms for side chain replacement, providing the necessary diversity to custom design molecules to generate and test diverse pharmacophoric models for different receptors. In addition, the minor changes in side chain orientation with different metals offer an opportunity for subtle optimization of binding specificity not available through conventional organic chemistry. The main goal of this study was to examine the conformations of MAC scaffolds both in crystals and in aqueous solutions, and to explore the structural and functional diversity by inclusion of different metals with appended functional groups at selected positions. Analysis of binding results of a library of such geometrical probes of turn-recognition motifs can be used to deduce the three-dimensional requirements for molecular recognition.

Methods

Crystal structures of MACs

A total of 28 MAC crystal structures (Table 1 and Figure 2), were retrieved from the Cambridge Structure Database (CSD version 5.27, May 2006) and examined for the distribution of distances between carbon atoms (corresponding to the C_α to C_α in peptides), virtual torsion angles between C–H bonds (corresponding to the C_α–C_β to C_α–C_β in peptides), and virtual torsion angles between four potential substituted carbon atoms [corresponding to the $C_\alpha(i)$–$C_\alpha(i + 1)$–$C_\alpha(i + 2)$–$C_\alpha(i + 3)$ in peptides]. These crystal structures complexed with different metals were used as a prototypical database of potential side chain orientations. We compared these geometrical features of MACs to a library of β-turn motifs, including 2736 Type I, 980 Type II, 482 Type I′, and 211 Type II′ β-turns, found in a representative list of high-resolution crystal structures of proteins.

Solvated structures of MACs

Here, we tried to elucidate the conformational preferences of two parent unsubstituted MAC scaffolds: one was the metal complexes of 1,4,7,10,13-pentaazacyclopentadecane (**I**, [M([15]aneN$_5$)]) and the other was the metal complexes of 3,6,9,12,18-pentaazabicyclo[12.3.1]octadeca-1(18),14,16-triene (**II**, [M(pyridin[15]aneN$_5$)]). These metal complexes might have alternative conformations in solution compared wirh those seen in crystals. For example, one of the complexes, **I**, with Mn^{2+} (**1**, PIHWEI) was prepared and crystallized as a 7-coordinate *trans-bis*-chloro structure, and the other X-ray structure of the bis(nitrate) derivative of **I** with Mn^{2+} (**2**, NAYSEL) revealed a 6-coordinate structure with a folded conformation of the pentaazacrown ring. Both of them behaved as a 1 : 1 electrolyte in methanol and 2 : 1 electrolyte in water (18), consistent with either a solvated 6-coordinate [M(L)•H_2O] structure or a 7-coordinate [M(L)•$(H_2O)_2$] structure in water. The

Table 1: Metal complexes of chiral azacrowns compounds complexed with different metals

Metals	CSD refcodes
Mn^{2+}	PIHWEI, NAYSEL, TOJVAP, NAYSAH, RUGZOI, XIDNUT, XIDNON, GABPOO, FARLAM, FEVGOD
Fe^{3+}	PURWUU, CEFMUV, AZOXAO, AMZOFE, FEPZOD, TAPIFE
Co^{2+}	INAXAW, COCLZP
Ni^{2+}	JISTEK, HABKOK
Cu^{2+}	MPZCUP, MOBDEM
Zn^{2+}	FUBTIF, UNAGIZ, HAHZAS, COTLUS, UHOFEC, OBEVOH

6-coordinate structure was also seen in the crystal structures of derivatives of complex **I** with Ni^{2+} (**19**, JISTEK; and **20**, HABKOK) and of derivatives of complex **II** with Mn^{2+} (**6**, XIDNUT) or Co^{2+} (**18**, COCLZP). As six is the most common co-ordination number among many metals, we primarily examined the 6-coordinate-solvated structures using DFT calculations as explicitly represented by interaction with an axial water ligand, and compared them with a 7-coordinate *trans-bis*-aquo structure with a planar pentaazacrown conformation.

All DFT calculations were done with the hybrid B3LYP method, as implemented in the GAUSSIAN03 program. Double-ζ and triple-ζ quality basis sets proposed by Ahlrichs and co-workers (29,30) were employed for non-metal and metal atoms, respectively. The crystal structures were taken as the starting points for geometry optimization. To avoid optimization trapped in local minima, multiple crystal structures (10 for **I** and 7 for **II**) were chosen as starting points. Only the structural minima with lowest energies are reported.

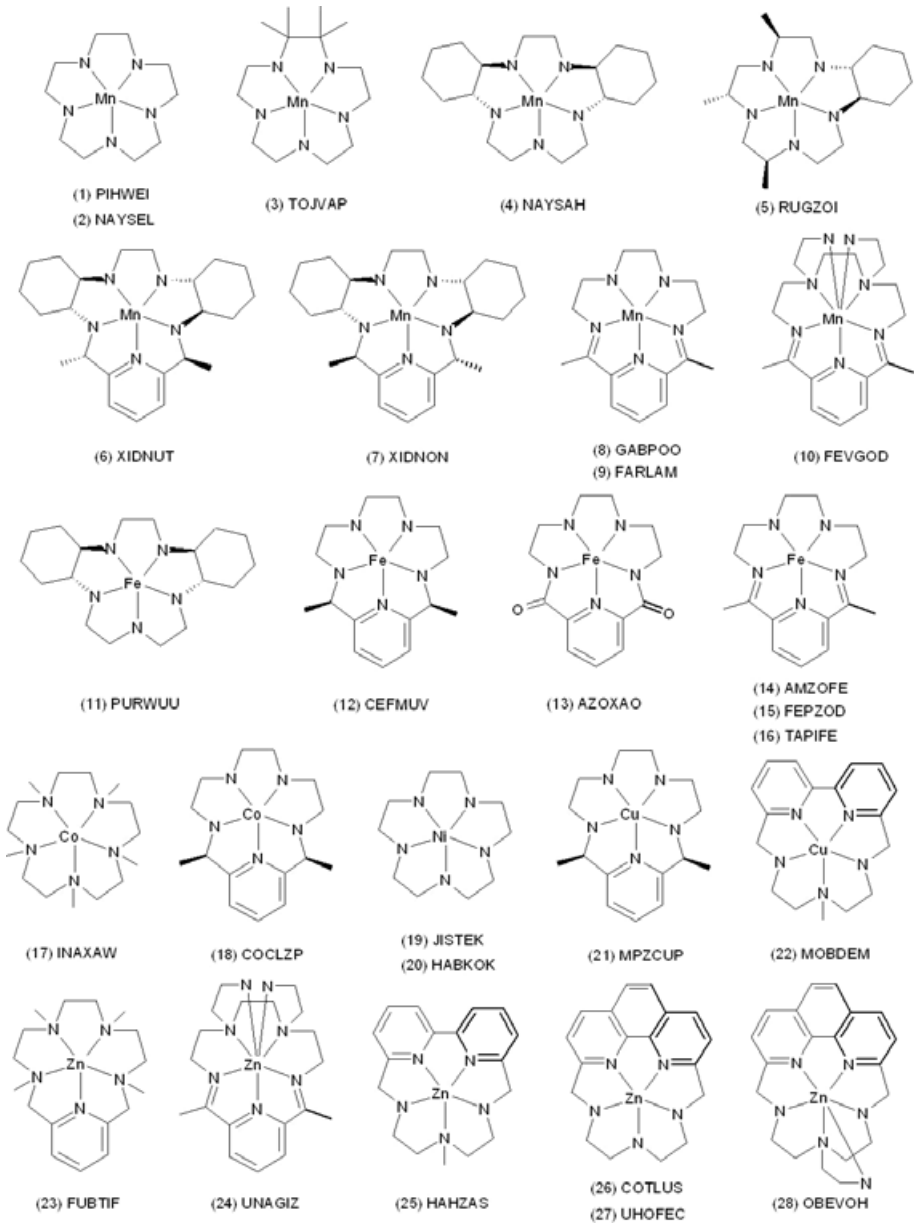

Figure 2: Chemical structures of 28 MACs complexed with 6 different metals. Most macrocyclic ligands were capped in the axial positions, usually with 0-2 counterions present which are omitted here for clarity.

Structural diversity of MAC scaffolds

To quantify structural diversity and information content accessible through MAC scaffolds, we followed a method developed in our previous study (31) employing principal component analysis (PCA). The spatial relationships (distance, angles, and virtual torsion angles) of C_α–C_β vectors of all tetrapeptide motifs found in a representative list of high-resolution crystal structures of proteins were subjected to PCA. The model was based on approximately 100 000 tetrapeptide structures. A similar calculation was carried out on MAC scaffolds with different patterns of substitutions as new sets of virtual C_α–C_β vectors. The PCA provides an easy way to visualize structural diversity and to compare MAC scaffolds with protein-structural epitopes and other peptidomimetic templates.

Results and Discussion

Crystal structures of MACs

Crystal structures of 28 MACs complexed with six consecutive metals in the periodic table (Mn to Zn) were retrieved from CSD for statistical analysis. The most common oxidation states for Mn to Zn are +2, except for Fe, which is +3. The exact oxidation state for each MAC compound as shown in Table 1 was checked with the original publications. The distributions of selected geometrical parameters of MACs are illustrated in Figure 3 and compared with those of β-turn motifs as illustrated in Figure 4.

The distance measured between carbons three atoms away (corresponding to the C_α–C_α distance in peptides) in the crystal structures of MACs ranges from 3.0 to 4.0 Å, with 83.5% within 3.6–3.9 Å, overlapping the relatively fixed C_α–C_α distance (3.8 Å) in peptides with *trans*-amide bonds. About 13% of distances between carbons in MACs ranges from 3.0 to 3.3 Å, closer to those of C_α–C_α distance (2.9 Å) involved a *cis*-amide bond, often observed in type VI β-turns. In pentaazacrowns, these shorter carbon–carbon distances often coincide with one carbon atom adjacent with one nitrogen donor which folds to occupy a pseudo-axial co-ordination position. The distance between carbons concentrated within a small range suggesting that the complexation with metals had effectively restricted the rotation around the CH_2–NH bond in pentaazacrowns, similar to those observed in peptides with amide bonds.

For molecular recognition, one of the most important features of the β-turn is the relative disposition of the four C_α–C_β bonds of residues i through $i + 4$ of the reverse turn. The C_α–C_β bonds of residues $i + 1$ and $i + 2$ of a β-turn motif are important because they govern the orientation of side chains of these two central residues, whose exposed nature make a logical recognition site. These two residues are often found as 'hot spots' for recognition of a β-turn motif. The virtual torsions between these two bonds, $C_\beta(i + 1)$–$C_\alpha(i + 1)$–$C_\alpha(i + 2)$–$C_\beta(i + 2)$, primarily ranged from 15° to 75° for both Type I (87.2%) and II (93.4%), and from −75° to −15° for both Type I′ (78.8%) and II′ (92.9%). The C_α–C_β bonds of residues i and $i + 3$ are also important because they determine the relative orientations of the other two side chains of the β-turn involved in recognition. The virtual torsions between the first two C_α–C_β bonds, $C_\beta(i)$–$C_\alpha(i)$–$C_\alpha(i + 1)$–$C_\beta(i + 1)$, primarily ranged from −135° to −45° for Type I (55.9%) and II (67.6%), and from −15° to 45° for Type I′ (58.5%) and II′ (60.2%); and the virtual torsions between the last two C_α–C_β bonds, $C_\beta(i + 2)$–$C_\alpha(i + 2)$–$C_\alpha(i + 3)$–$C_\beta(i + 3)$, primarily ranged from 45° to 135° for Type I (50.7%) and II (80.6%), with a very similar distribution for both Type I′ and II′, also from 45° to 135° for Type I′ (86.5%) and II′ (79.7%). Those corresponding virtual torsions between potential adjacent C_α–C_β bonds in MACs appeared to distribute almost evenly among all possible values, with the exception that those values between 45° and 75° and between −75° and −45° were twice that expected from an even distribution. These observations indicated that the relative orientations of the four C_α–C_β bonds involved in reverse-turn recognition may be reproduced with a subset of substitution patterns on MAC scaffolds.

Unlike α-helices and β-strands, the backbone conformation of β-turns makes almost a complete 180° reversal in the direction of their polypeptide chains. Hence, the overall topography of β-turns can in part be described in terms of a single virtual torsion between the four C_α-atoms, $C_\alpha(i)$–$C_\alpha(i + 1)$–$C_\alpha(i + 2)$–$C_\alpha(i + 3)$, which provides a complete description of the spatial relationship between the entry and exit peptide bonds as well as the relative orientations of the intervening side chains for any β-turns. They primarily ranged from −15° to 45° for Type I (95.7%) and II (97.0%), and from −75° to −15° for Type I′ (81.9%) and II′ (97.1%). Those corresponding virtual torsion angles in MACs were found to mainly scatter between −45° and 45° (82.6%), which appeared to coincide with the distribution of β-turn motifs. As a comparison, this virtual torsion angle would be around 50° and −160° for those in α-helices and β-strands, respectively. Therefore, the topographical features observed across a wide variety of MAC crystal structures with different metals proved that metal complexes of pentaazacrowns provided preferred templates reproducing the overall direction of reverse-turn motifs as well as the spatial relationship between their functionalized side chains.

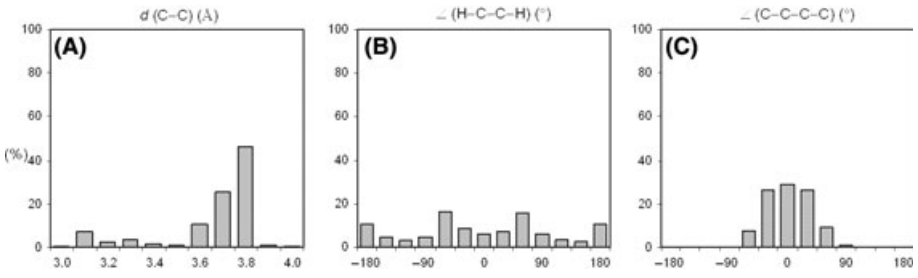

Figure 3: The distribution of geometrical parameters for 28 MAC crystal structures with 6 different metals: distances between carbon atoms (A), virtual torsion angles between C-H bonds (B), and virtual torsion between four potential substituted carbon atoms (C).

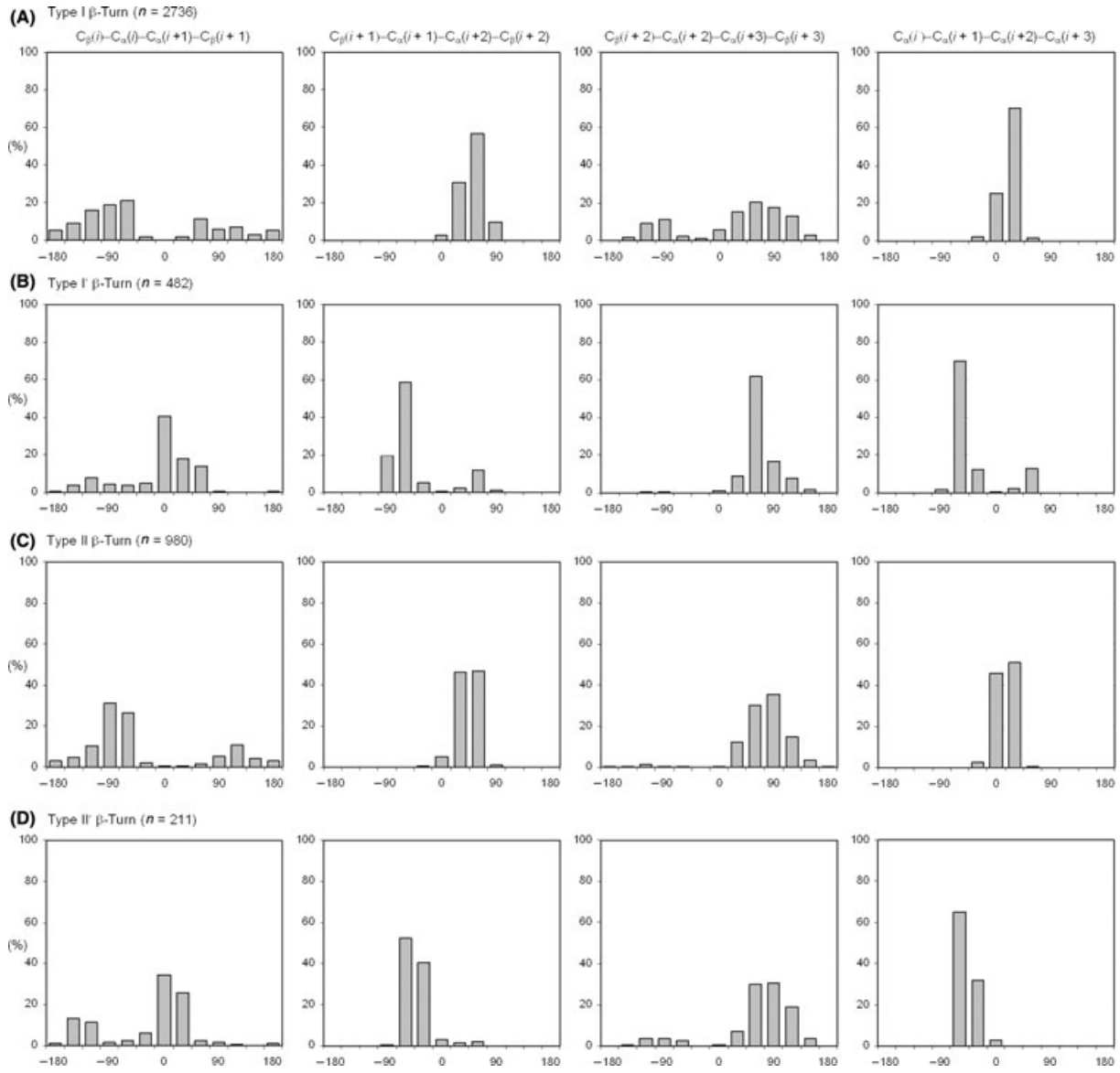

Figure 4: The distribution of virtual torsion angles (°) between adjacent C_α-C_β bonds and between peptide backbone Cα atoms for type I (A), type I′ (B), type II (C), and type II′ (d) β-turn motifs.

Solvated structures of MACs

The dissociative exchange rate of water on the metal complexes of pentaazacrowns had been previously estimated to be $\sim 0.8 \times 10^7$/s at pH 7 and 25 °C (18). Moreover, in aqueous solution, a dynamic equilibrium of 6- and 7-coordinate structures is expected, and the population distribution between the two conformations depends on chemical substitutions along the periphery of the pentaazacrown rings. As 6 is the most common co-ordination number for the studied metals and the 6-coordinate structures of pentaazacrowns complexed with Mn^{2+} is correlated the catalytic activity of superoxide dismutation (22), we mainly elucidated the 6-coordinate-solvated structures [M([15]aneN$_5$)•H$_2$O] (**I**) and [M(pyridin[15]aneN$_5$)•H$_2$O] (**II**) with one of the axial sites occupied by a water molecule. Further, different metals will perturb the pentaazacrown conformation in slightly different ways. To address such influences, six different metals (Mn^{2+} to Zn^{2+}) were considered in the current study. In addition, the impact of different oxidation states of metals was also evaluated with Mn^{3+}/Mn^{2+} and Fe^{3+}/Fe^{2+}. The pentaazacrown structures under study are illustrated in Figures 5–7 and the DFT calculation results are summarized in Tables 2–4.

Solvated structures of I, [M([15]aneN$_5$)•H$_2$O]

The 7-coordinate crystal structure of **I** (**1**) had a planar pentaazacrown conformation. The arrangement of the N–H bonds of the secondary amine donors is such that they alternate in their relative orientation to the plane generated by the five nitrogens and the central metal, i.e. the N–H bonds are arranged in an up-down-up-down-up stereochemistry, as illustrated in Figure 5. Thus, the two side of the pentaazacrown ring in the complex

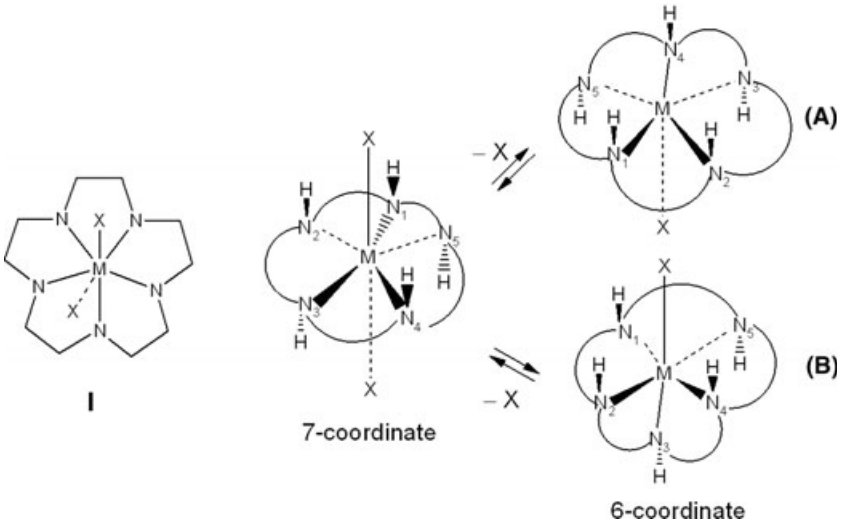

Figure 5: View of pentaaza macrocyclic ligand complex, $[M([15]aneN_5)X_2]$ (1), with a stereo depiction of the NH orientation. Only one possible 6-coordinate structure available generated via ligand dissociation from a 7-coordinate complex.

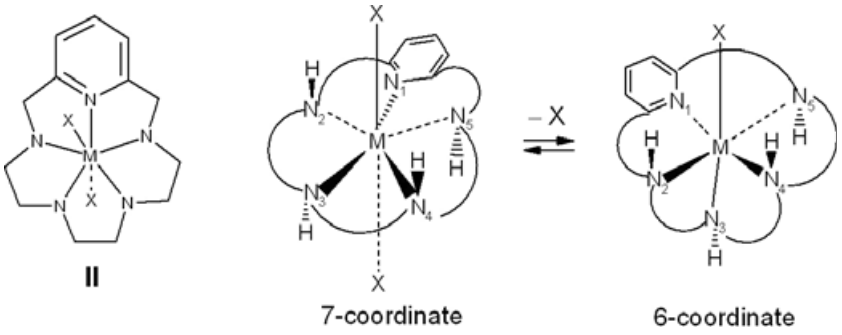

Figure 6: View of pentaaza macrocyclic ligand complex, $[M(pyridin[15]aneN_5)X_2]$ (2), with a stereo depiction of the NH orientation. Only one 6-coordinate structure generated via ligand dissociation from a 7-coordinate complex.

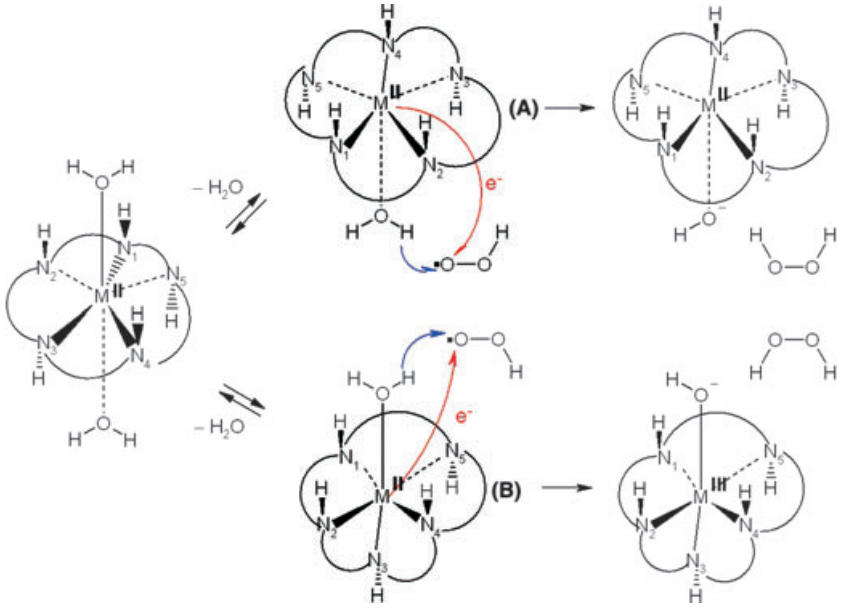

Figure 7: Mechanistic scheme depiction for the formation of a 6-coordinate complex which gives rise to the outer-sphere proton coupled electron transfer pathway for oxidation of Mn(II) and Fe(II) by perhydroxyl radical (protonated superoxide, $HO_2\bullet$).

are chemically distinct. One side of the plane of the pentaazacrown orients two non-adjacent N–H bonds, while the opposite side has three N–H bonds in a *cis*-orientation. This same pattern of N–H bonds has been seen in all X-ray crystal structures of pentaazacrown complexes determined so far. Therefore, two types of 6-coordinate structures could be generated via the loss of an axial ligand from the 7-coordinate structure, i.e. the complex labeled **A** in Figure 5, which has the vacant site on the

Table 2: DFT-optimized geometries for both of the possible 6-coordinate structures of pentaaza macrocyclic complex **1** with six different divalent metal ions and their relative energies [distance in Å, angle in °, and energy in kcal/mol; the axial ligand (X) is a water molecule]

Metal	Conformation	d(M–X)	d(M–N_1)	d(M–N_2)	d(M–N_3)	d(M–N_4)	d(M–N_5)	<X–M–N_1	<X–M–N_2	<X–M–N_3	<X–M–N_4	<X–M–N_5	ΔE (A − B)
Mn^{2+}	A	2.430	2.336	2.277	2.325	2.295	2.292	103.4	89.3	85.4	132.7	80.6	+3.06
	B	2.340	2.298	2.348	2.326	2.307	2.318	87.8	88.8	140.7	86.1	105.4	
Fe^{2+}	A	2.572	2.285	2.220	2.272	2.247	2.228	95.4	84.7	88.0	136.7	76.3	+3.02
	B	2.393	2.225	2.291	2.271	2.243	2.272	82.1	93.1	148.0	83.2	93.5	
Co^{2+}	A	3.612	2.213	2.184	2.171	2.174	2.167	120.9	102.4	58.8	95.8	57.5	−0.04
	B	2.415	2.186	2.259	2.226	2.208	2.218	82.7	85.2	141.1	81.3	100.0	
Ni^{2+}	A	3.726	2.168	2.157	2.125	2.121	2.119	123.6	103.2	55.7	96.3	54.3	−0.11
	B	2.363	2.096	2.192	2.188	2.134	2.127	83.1	89.4	163.6	88.0	94.0	
Cu^{2+}	A	3.747	2.099	2.089	2.075	2.242	2.225	126.4	106.1	53.2	93.0	56.0	−0.91
	B	4.042	2.061	2.121	2.298	2.222	2.097	42.0	88.5	169.4	105.4	81.2	
Zn^{2+}	A	3.699	2.232	2.189	2.189	2.159	2.158	122.5	104.1	56.9	96.4	55.4	−1.55
	B	2.954	2.145	2.250	2.209	2.140	2.260	73.7	86.7	146.0	75.7	92.6	

Table 3: DFT-optimized geometries for the 6-coordinate structures of pentaaza macrocyclic complex **2** with six different divalent metal ions [distance in Å and angles in °; the axial ligand (X) is a water molecule]

Metal	d(M–X)	d(M–N_1)	d(M–N_2)	d(M–N_3)	d(M–N_4)	d(M–N_5)	<X–M–N_1	<X–M–N_2	<X–M–N_3	<X–M–N_4	<X–M–N_5
Mn^{2+}	2.283	2.204	2.352	2.320	2.307	2.323	90.4	91.8	146.4	88.4	102.5
Fe^{2+}	2.241	2.158	2.298	2.272	2.263	2.253	84.7	91.3	151.9	89.7	97.8
Co^{2+}	2.253	2.103	2.255	2.229	2.224	2.226	86.6	91.3	154.4	87.8	99.4
Ni^{2+}	2.258	2.048	2.240	2.179	2.180	2.155	84.4	91.6	160.5	87.6	94.9
Cu^{2+}	3.739	1.966	2.077	2.199	2.186	2.106	107.1	52.8	93.5	56.6	129.8
Zn^{2+}	2.428	2.094	2.252	2.229	2.175	2.270	84.4	86.9	148.7	82.9	99.2

Table 4: DFT-optimized geometries for both of the possible 6-coordinate structures of pentaaza macrocyclic complex **1** with trivalent metals, Mn(III) and Fe(III) [distance in Å and angle in °; the axial ligand (X) is a hydroxide ion]

Metal	Conformation	d(M–X)	d(M–N_1)	d(M–N_2)	d(M–N_3)	d(M–N_4)	d(M–N_5)	<X–M–N_1	<X–M–N_2	<X–M–N_3	<X–M–N_4	<X–M–N_5
Mn^{3+}	A	1.791	2.443	2.295	2.274	2.176	2.166	102.4	88.7	88.7	142.6	91.5
	B	1.795	2.245	2.300	2.170	2.180	2.420	93.2	82.6	158.7	94.0	95.5
Fe^{3+}	A	1.784	2.317	2.258	2.319	2.298	2.347	107.9	95.2	89.0	117.6	88.6
	B	1.782	2.321	2.277	2.290	2.367	2.280	93.0	93.9	126.3	89.0	101.9

side in which three N–H bonds are *cis*, and the structure labeled **B**, which has the vacant site on the side with two non-adjacent N–H bonds. Clearly, the two 6-coordinate structures **A** and **B** are chemically quite distinct.

The DFT calculations revealed a planar pentaazacrown conformation for the 7-coordinate structure of **I** complexed with Mn^{2+}. The metal ion was seven co-ordinate with a pentagonal bipyramidal co-ordination geometry in which the water ligands lie in *trans* sites above and below the plane of the pentaazacrown. The distance between the Mn^{2+} ion and the two axial water ligands, d(Mn^{2+}–O), were 2.395 and 2.588 Å with the water molecules on the side of the three N–H bonds having a shorter distance. This suggested that structure **B** was likely the preferred 6-coordinate conformation. The bond angle around the Mn^{2+} ion, ∠O–Mn–O, was 174.4° close to the 178.9° bond angle observed in the *trans-bis*-chloro crystal structure (**1**). The Mn–N bond lengths were found to vary between 2.339 and 2.420 Å. This relatively small variation in bond lengths suggested that the high-spin Mn^{2+} was well accommodated within the pentaazacrown cavity. The N–Mn–O bond angles were observed to range from 80.9° to 108.9°, indicating the five nitrogens and the metal were approximately coplanar.

For the two chemically distinct 6-coordinate structures with Mn^{2+}, structure **B** with the axial water ligand on the side of three N–H bonds was found to be 3 kcal/mol more stable than structure **A**. Both **A** and **B** adopted a 6-coordinate distorted octahedral geometry with one of the nitrogens of the pentaazacrown folded to occupy a pseudo-axial co-ordination position of an octahedron, i.e. structure **A** with an NH group from the side of the three N–H bonds folding into an axial O_h site, and structure **B** with an NH from the side of two N–H bonds folding into the axial octahedral co-ordination site. The resultant N–Mn–O bond angle involving the folded nitrogens was 132.7° and 140.7° for **A** and **B**, respectively. These structures are seemingly intermediate between the planar pentaazacrown conformation and a folded array with the idealized N–Mn–O bond angle of 180°. Thus, while the structures were distorted from true octahedral, the ligand adopted a folded geometry in which one of the nitrogens was considerably displaced from the plane of the Mn^{2+} ion and the remaining four nitrogens. The

distance between the Mn^{2+} ion and the remaining water ligand, Mn–O, was 2.430 and 2.340 Å for **A** and **B**, respectively. Both of the Mn–O bond lengths were shorter than the corresponding ones in the 7-coordinate structure. Similarly, the Mn–N bond lengths in both **A** and **B** were also somewhat shorter than those observed in the 7-coordinate structure, i.e. the Mn–N bond lengths were found to vary between 2.277 and 2.336 Å and between 2.298 and 2.348 Å in **A** and **B**, respectively. In addition, structure **B**, the relatively more folded conformation, had a slightly shorter Mn–O bond length and a larger average Mn–N bond length than those of structure **A**.

Inclusion of the other five metals (Fe^{2+}, Co^{2+}, Ni^{2+}, Cu^{2+}, and Zn^{2+}) as pentaazacrown complexes led to several minor-to-significant changes in the solvated structures of **I**. The energetic differences between structures **A** and **B** varied between different central metals, both in sign and magnitude. Complex **I** with Fe^{2+}, like Mn^{2+}, also preferred structure **B** by about 3 kcal/mol. The magnitude of the difference (0.04 and 0.11 kcal/mol) was negligible for complexes with either Co^{2+} or Ni^{2+}. Structure **A** would be favored by about 0.91–1.55 kcal/mol in the complexes with Cu^{2+} and Zn^{2+}. Clearly, the DFT results suggested that the pseudo-octahedral structure **A** was increasingly favored as the nuclear charge of the metal increased. This trend may be partially due to the differences in the binding energies for the two axial water ligands. We have determined the binding energies for the leaving axial water with DFT and corrected them for the basis set superposition error (BSSE) by the counterpoise method. In the Mn^{2+}-complex of **I**, the binding energy for the water molecule on the side of three N–H bonds (the loss of this axial water ligand leads to structure **A**) was estimated to be about 13.0 kcal/mol, and the binding energy for the other axial water was 17.1 kcal/mol. The binding energy for the first water increased gradually to 15.7 kcal/mol in the Zn^{2+}-complex; in contrast, the binding energy for the second water decreased gradually to 13.0 kcal/mol. The Fe^{2+} ion caused a slightly more folded structures than those of Mn^{2+}, i.e. the resultant N–Fe–O bond angle were 136.7° and 148.0° in structures **A** and **B**, respectively. The distance between the Fe^{2+} ion and the axial water ligand was 0.053–0.142 Å greater than those of Mn^{2+}-complexes.; while, the average Fe^{2+}–N bond length (2.255 Å) was slightly shorter than the average Mn^{2+}–N bond length (2.312 Å). Both the Co^{2+}- and Ni^{2+}-based pentaazacrowns have structure **A** with a significant larger distance between the metal ions and the water molecules, 3.612 and 3.726 Å, respectively. The average distances between the metal and the nitrogen donors were 2.201 and 2.143 Å for the Co^{2+}- and Ni^{2+}-based complexes, respectively. The **B** structure of the Ni^{2+}-complex had a conformation most close to true octahedral among all the studied compounds, with an N–Ni^{2+}–O bond angle of 163.6°. The pentaazacrowns with Cu^{2+} revealed a pseudo-trigonal bipyramidal geometry with two NH groups occupying two sites which approximate *trans*-positions in a trigonal bipyramidal structure. Both of structures **A** and **B** of the Cu^{2+}-complexes had a much larger distance (3.747 and 4.042 Å) between the metal and the remaining water molecule. The average Cu^{2+}–N bond length was 2.153 Å. The 6-coordinate conformations of pentaazacrowns with Zn^{2+} were somewhat similar to those of Co^{2+}- and Ni^{2+}-complexes. The average Zn^{2+}–N bond length was estimated to be 2.193 Å.

The DFT results on the 6-coordinate structures of pentaazacrowns, particularly the conformational preference for structures **A** and **B**, were consistent with a number of previous experimental observations. For example, the X-ray crystal structure determination of *bis*(nitrate) derivative of **I** complexed with Mn^{2+} (**2**) revealed a 6-coordinate structure with a folded conformation of the pentaazacrown ligand with the resultant N–Mn–O bond angle of 132.0°. The crystal structure with the nitrate ligand on the side of three NH groups was consistent with structure **B**. The crystal structures of **I** complexed with Ni^{2+} also indicated a 6-coordinate geometry with the axial site occupied by either a water molecule (**19**) or a perchlorate ion (**20**). Both of them were consistent with structure **B**. In contrast, the crystal structure of the all *N*-methylated derivative of **I** complexed with Co^{2+} (**17**) disclosed a structure compatible with structure **A**. Previously, Riley *et al.* (22) have probed the relative energetics of the two types of 6-coordinate structures using molecular mechanic (MM) calculations employing the CAChe system. The code was based on Allinger's MM2 force field with extensions and metal parameters provided by the CAChe group. In contrast to the DFT results, for all considered pentaazacrowns compounds with Mn^{2+}, structure **A** was found to be at a much lower energy than structure **B**, in the range of 4–8 kcal/mol for chloro as axial ligand and 8–12 kcal/mol for the aquo complex. More importantly, Riley *et al.* (22) used the same MM approach and predicted correctly that certain substitutent patterns and substituents of manganese complexes of pentaazacrown would enhance or reduce the catalytic rate of superoxide dismutation. In addition, it is of interest to note that one complex with Mn^{2+} (**5**) crystallizes with a water at one co-ordination site *trans* to a chloro ligand. Further, the water is bound on the side of the macrocycle that possesses two *cis* non-adjacent NH groups and the chloro ligand on the side with the other three NH groups. In other words, if the chloro ligand dissociated from the compound, it would lead to a 6-coordinate structure consistent with structure **A**. As the two sides of the pentaazacrowns in the complex are chemically distinct, the distance between the metal and the two axial ligands should be different, which may indicate which ligand is more likely to dissociate from the complex. It was found that in the *trans-bis*-chloro complexes of **1** and **4**, the chloro ligand on the side of two NH groups was closer to the metal center than those on the other side (2.571 versus 2.635 Å and 2.560 versus 2.631 Å); however, in the complexes of **3** and **8**, the opposite relationship in the metal–ligand bond length was observed (2.696 versus 2.606 Å and 2.349 versus 2.329 Å). Further experimental and computational studies are needed to address the relative energetics and the dynamic equilibrium between the 6- and 7-coordinate structures.

It was anticipated that the average distance between carbons 3 atoms away (corresponding to C_α–C_α in peptides) on the pentaazacrowns would increase with the ionic radius of the metal. In other words, the cavity of the pentaazacrown would change to accommodate different metals. The DFT calculations revealed the average distance between these carbons ranging from 3.579 to 3.660 Å, having a strong correlation ($R^2 = 0.96$) with the metal ionic radius of Shannon (32), as depicted in Figure 8. It was estimated that a distance ranging from 2.95 to 3.95 Å would be observed between these carbons on the pentaazacrowns if the rotation was unimpeded around the central CH_2–NH bond. This offers an upper/lower limit of the size of metal that a pentaazacrown could accommodate. Hence, a metal with an ionic radius above 1.43 Å would be too large for the current penta-

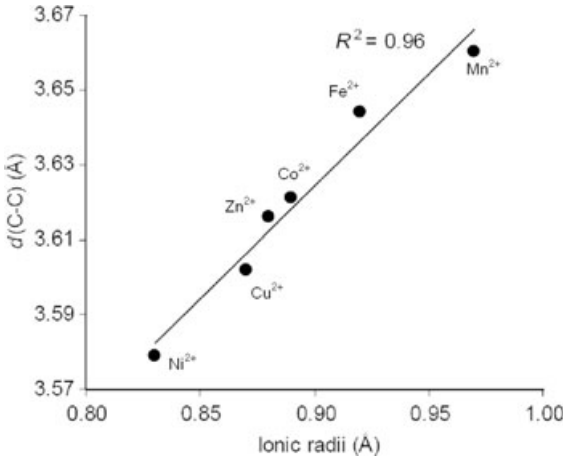

Figure 8: The average distances (Å) between carbons 3 atoms away (corresponding to C_α-C_β in peptides) of MACs increase linearly (R^2 = 0.96) with the metal ionic radii (Å) of Shannon (32).

azacrown template. On the other hand, pentaazacrowns complexed by a metal with an ionic radius of about 1.18 Å (such as the lanthanides) would show an average distance between carbons 3 atoms away of about 3.80 Å, close to those seen in proteins.

Solvated structures of II, [M(pyridin[15]aneN$_5$)•H$_2$O]

A simple way to overcome the uncertainty in the 6-coordinate structure was to incorporate a pyridine ring into the pentaazacrown ring. There are even number of NH groups, thus, the two sides of the plane, defined by the metal and the five nitrogens, are chemically equivalent. The crystal structures of this class also revealed both 7- and 6-coordinate structures, all possessing an alternating up-down-up-down N–H orientation. Another benefit of **II** was an improved stability profile when compared with those of **I**. An excellent example was seen in the manganese complex of **II**, which was nearly 175 times more kinetically stable at any pH than the manganese complex of **I** (19). Such enhancement is undoubtedly due to in part from the rigidity conferred on the ligand by the pyridine substitution; the most important factor can be attributed to the much lower basicity of a pyridine (p*K*a = 5.42) compared with a secondary amine (p*K*a = 10.73). In addition, the complex **II** has only 16 H-atom sites that could be chirally substituted along the periphery of the pentaazacrown, compared with 20 sites on complex **I**. It is possible, however, to introduce additional functional groups on the pyridine to enhance the molecular diversity of this template.

The DFT results suggested that the optimized 6-coordinate geometries of **II** were similar to those of seen in the complexes of **I**, particularly structure **B**. They adopted a distorted octahedral geometry with a water occupying an axial ligand site, except for the complex with Cu^{2+} having a large distance between water and the copper ion and showing a pseudo-trigonal bipyramidal structure. The resultant N–M–O bond angles involving a folded NH group were found to be close of those values seen in structure **B** of complex **I**. In addition, the distances between the metal ion and the axial water ligand were all shorter than those observed in **I**. Furthermore, the distance between the pyridine nitrogen and the metal was consistently shorter than the rest of metal–nitrogen distances.

Oxidation/reduction of MACs

Metal complexes can undergo oxidation/reduction reactions under certain conditions. For example, manganese complexes of pentaazacrowns have been developed as SOD mimetics, in which the manganese moiety functions in the dismutation reaction of superoxide anions by successive reduction followed by oxidation changes in its valence between Mn^{2+} and Mn^{3+}, in analogy with native SODs. The major catalytic mechanism of these enzyme mimetics involves a proton-dependent pathway, in which oxidation of an aquo-Mn^{2+}-complex to Mn^{3+}(hydroxo) by perhydroxyl radical (protonated superoxide) occurs via an outer-sphere proton-assisted electron transfer, i.e. H-atom transfer, as illustrated in Figure 7. The resting oxidation state of the complex is the reduced Mn^{2+} ion, which is very stable due to the high-spin d^5 electronic configuration. As the complex is very difficult to oxidize, many one-electron oxidants, including nitric oxide and oxygen, are ineffective. Further, as these complexes operate through a facile one-electron oxidation pathway, other two-electron non-radical, but nevertheless, potent oxidants, such as peroxynitrite, hydrogen peroxide, or hypochlorite, are not kinetically competent to oxidize the Mn^{2+}-complex. In addition, the corresponding iron derivatives were also investigated as SOD mimetics. As with the Mn^{2+}-complex, the stable oxidation state of the complex is that which favors the high-spin d^5 electronic configuration. Thus, in aqueous solution at pH 7.4, the iron complexes exist predominantly as their Fe^{3+}(hydroxo) complexes. Here, DFT calculations were also carried out on the Mn^{3+}(hydroxo) and Fe^{3+}(hydroxo) complexes of **I** to probe the impact of such changes in oxidation states on the conformations of pentaazacrowns. Their results were summarized in Table 4.

Significant conformational changes in pentaazacrowns were seen computationally with oxidation of both Mn and Fe complexes. The characteristic N–Mn–O bond angles increased from 132.7° and 140.7° of the Mn^{2+}(aquo) complex to 142.6° and 158.7° of the Mn^{3+}(hydroxo) complex for structures **A** and **B**, respectively. On the other hand, the characteristic N–Fe–O bond angles decreased from 136.7° and 148.0° of the Fe^{2+}(aquo) complex to 117.6° and 126.3° of the Fe^{3+}(hydroxo) complex for structures **A** and **B**, respectively. This difference can be attributed to the electronic configurations of the metal ions and the corresponding ligand field effects. Both of the Mn^{2+}- and Fe^{3+}-complexes in this study having high-spin d^5 electronic configurations that are not subject to ligand field effects, thus each metal complex possesses a spherically symmetrical *d*-electron distribution. For metals with ligand field effects, such as Mn^{3+} and Fe^{2+} with high-spin d^4 electronic configurations, an octahedral ligand environment would be induced if possible for the ligand. It is conceivable that such geometrical differences in pentaazacrown geometry could be exploited with switchable receptor binding on oxidation/reduction, for example, a MAC of Mn^{2+} could orient side chains relatively more planar and when oxidized to Mn^{3+}, an octahedral complex would result with one nitrogen co-ordinated in an axial position, thus altering receptor affinity/selectivity of the MAC.

Structural diversity of MAC scaffolds

Proteins are one of nature's ways of creating high level of molecular diversity through different types of amino acids constrained by secondary and tertiary conformations. Thus, molecular diversity of proteins can be split into a functional part (types of side chains) and a

geometrical part (relative orientation of the side chains). These geometrical orientations are defined by C_α–C_β bonds that link the side chains to the backbone. This split of molecular diversity can also be applied to peptidomimetic scaffolds, merely serving to control the relative orientation of the functional groups that make only a small contribution to the biologic property of the compound. MACs are able to offer tremendously diverse orientations of side chains through different substitution patterns. For example, there are 20 H-atom sites along the periphery of the pentaaza macrocycle of **I** that could be chirally substituted. Considering only single substitution between two adjacent NH groups, $5 \times 4^4 = 1280$ unique compounds are possible, all with similar molecular properties due to the same molecular weight and same type of side chain, but with different relative orientations. In addition, the possible minor-to-significant changes in orientation of side chains with different metals/oxidation and spin states and a number of chemical modifications of the macrocyclic rings offer additional structural diversity accessible to MAC scaffolds. This diversity gives chemists sufficient scope to design compounds to fit a unique pharmacophoric model, and should lead to rapid identification of spatial requirements from compounds active in screening of diverse MAC libraries.

Previously, the PCA was used to analyze the spatial relationships of C_α–C_β bonds of tetrapeptides to estimate the information content and quantify and compare structural diversity of peptides and peptidomimetic scaffolds (31). The PCA model, based on geometrical properties of approximately 100 000 tetrapeptides, was discussed in details therein, including the coefficients and loadings of each field and the proportion of variance explained by each principal component. The model yielded two optimal principal components, according to a conservative statistical rule of thumb that attributes significance only those components having eigenvalues >1, i.e. those explaining at least as much of the overall data variance as did one of the original variables. The first component, PCA1, with an eigenvalue of 7.22 reproduced 60.2% of the original variance in all tetrapeptides. Its combination with the second principal component, PCA2, with an eigenvalue of 1.24 reproduced 70.5% of the original variance. PCA1 strongly correlated with the distance between the first and last C_α-atoms, mainly describing the compactness of tetrapeptides; therefore, α-helices (the most compact secondary structure) were clustered to the left with smaller scorings of PCA1, β-strands (the most extended secondary structure) were clustered to the right, and turns were distributed in the middle. PCA2 more correlated with the distances between adjacent C_α-atoms, mainly accounting for local geometry of tetrapeptides, such as *cis*- or *trans*-amide bonds. For example, type VI β-turns with a *cis*-amide bond between the second and third residues, having scorings of PCA2 ranging from −20 to −15, were scattered well separated from other β-turn motifs or any other regular secondary structures with *trans*-amide bonds.

A similar analysis was carried out on MAC scaffolds (**I**; 6-coordinate-solvated structures complexed, with six different metals), and their scorings were illustrated in Figure 9. The comparison suggested that more than half of the spatial orientations of side chains of β-turn motifs were closely mimicked with a subset of substitution patterns on the scaffolds studied. These MAC scaffolds covered very little of the space accessible to α-helices and β-strands, emphasizing their utility for chemical libraries only relevant to reverse-turn conformations. However, β-turn motifs with scorings of PCA2 >1.5 were almost absent of their MAC scaffold counterparts. This may partially due to the relatively smaller distances between carbons three atoms away in MACs (mean values range from 3.58 to 3.66 Å complexed with Mn^{2+} to Zn^{2+}; see Figure 8) compared with those of C_α to C_α distances (3.80 Å) in peptides. The inclusion of metals with larger ionic radii can hopefully in part increase the distances between carbons 3 atoms away in MACs, therefore, increase the scorings of PCA2, as exemplified in the crystal structure $[Cd([15]aneN_5)Cl_2]$ with an average carbon distances of 3 atom away of about 3.72 Å (the ionic radius of Cd^{2+} is about 1.09 Å). Many other metals with both smaller/larger ionic radii and important therapeutic applications would be extremely useful to enhance the structural space accessible to MACs, such as Gd^{3+} (1.08 Å) widely used as a MRI agent, $^{99m}Tc^{4+}$ (0.79 Å), $^{64}Cu^{2+}$ (0.87 Å), and $^{111}In^{3+}$ (0.94 Å) with diverse applications in radiopharmaceutical chemistry for positron emission tomography. These results are exceptionally encouraging for developing a 2D library of chiral MACs complexed with different metals to further probe the subtle details of receptor recognition.

Further, we developed a simple criterion, based solely on the scorings of PCA1 and PCA2, to quantitatively evaluate the impact of different metals on β-turn mimicry. If a quad substitution pattern had a value of PCA1 between −1 and +1 and a value of PCA2 between −3 and +3, we considered it a hit for a potential β-turn motif. For MAC scaffold **I**, there were 181 hits when complexed with Mn^{2+}, 96 for Fe^{2+}, and 62 for Co^{2+}. There were less for the other three, 10 for Ni^{2+}, 15 for Cu^{2+}, and 30 for Zn^{2+}. This trend may in part due to two factors. One is the ionic radii of metals as discussed above. The number of hits is clearly correlated with the size of ionic radii ($R^2 = 0.92$). Mn^{2+} has the largest ionic radius of the studied metals and is also associated with the largest number of hits for β-turn motifs. And the other factor is the ligand conformations of pentaazacrown rings. A planar ligand conformation is usually associated with more hits than those of folded structures. For example, 109 and 125 hits were observed for

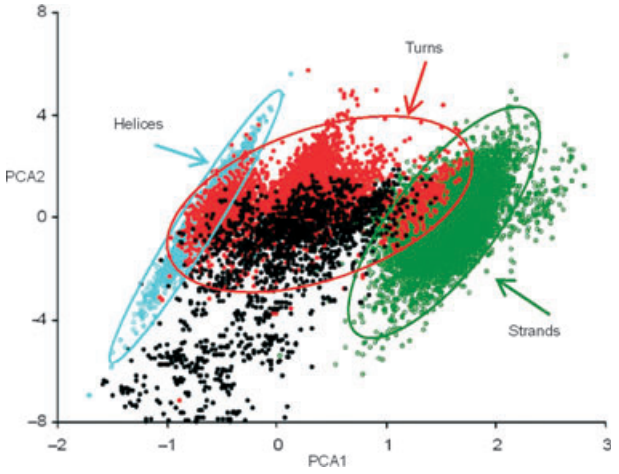

Figure 9: The structural diversity accessible through protein surfaces and MAC scaffolds. Each point represents a set of four sequential C_α-C_β bonds in peptides or those derived from appending substituents to a scaffold. Helices in blue, strands in green, turns in red, and MACs in black.

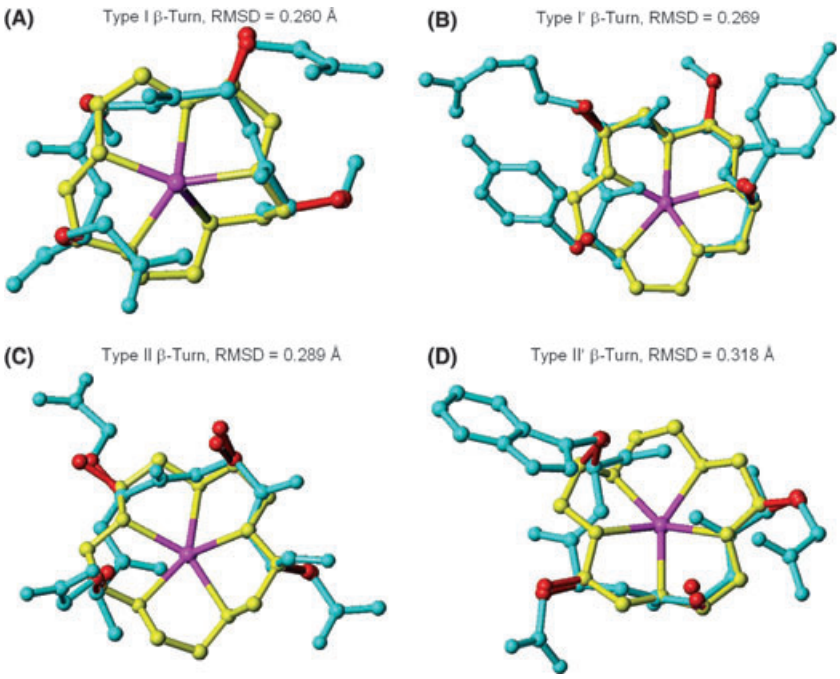

Figure 10: Overlaps of MACs with different types of β-turn motifs: type-I turn (Ser-Glu-Ser-Gln, PDB: 1D5T[396-399]) (A), type-I′ turn (Tyr-Arg-Ser-Tyr, 1QDD[21-24]) (B), type-II turn (Glu-Glu-Gly-Asn, 1W0H[18-21]) (C), and type-II′ turn (Glu-Gly-Asp-Trp, 1IUA[55-58]). MACs in yellow, β-turn motifs in cyan, and the superimposed side chains in red, respectively. The metal, Mn(II), is shown in center with the axial ligands omitted for clarity.

Mn^{3+} and Fe^{3+}, respectively, which reflects the fact that Mn^{2+} or Fe^{3+} in the high-spin d^5 electron configuration without subject to ligand field effect prefers a relatively planar ligand arrangement compared with those of Mn^{3+} or Fe^{2+}. When comparing the relative spatial locations of the chiral side chains, a strong overlap with β-turn structures in native proteins was observed for many substitution patterns, with an RMSD of only 0.3 Å for all four C_α–C_β bonds. Selected examples of mimicking the most common β-turns, Type I and II, and their mirror images (of the backbone, but not the side chains), Type I′ and II′, using MAC scaffold **I** complexed with Mn^{2+} are illustrated in Figure 10.

Conclusions

In the postgenomics era, the exponential increase in potential therapeutic targets is placing an ever-increasing demand on novel and diverse chemical libraries. Peptides, or small domains of proteins, dominate vast molecular interactions in biologic systems. However, the chemical structure of peptides lead to degradation in biologic systems limiting oral bioavailability. Peptidomimetics, more drug-like structures that interact with peptide receptors, are sought through combinatorial chemistry and high-throughput screening. For modulating protein–protein interactions, peptidomimetic scaffolds that closely resemble surfaces of protein-recognition motifs can be privileged in a chemical sense; in other words, the chemical space accessible to the scaffold is effectively complementary to the biologic space. Rapid access to privileged scaffolds should provide not only improved hit discovery, but also more efficient hit-to-lead development. Turns, the most common type of non-repetitive motifs in proteins, have frequently been implicated as protein-recognition sites. This study focuses on the peptidomimetic development and tailoring structural and functional diversity in a library through MACs. Both of the crystal and solvated structures of MACs have demonstrated that MACs provide preferred templates closely resembling the overall direction of reverse-turn motifs as well as the spatial locations of side chains. In addition, structural comparisons have confirmed that the potential orientations of side chains through chiral substation of MACs are in close agreement with those of many β-turns seen in proteins. The subtle changes in the spatial arrangement of functional groups with complexation of different metals offer an exceptional opportunity for optimization of binding affinity/specificity not available through conventional organic chemistry. The MAC chemical library with systematically altered shapes and surfaces by the use of different metals, substitution patterns, and chemical modifications on the macrocyclic ring will facilitate the determination of the receptor-bound conformation in combination with the variety of other peptidomimetic scaffolds currently in use.

Acknowledgments

This research was supported in part by the Intramural Research Program of the NIH, NHLBI (BRB), and an NIH research grant (GM 68460) to GRM. Y.C. also acknowledges a postdoctoral research fellowship from the National Heart, Lung and Blood Institute. This study utilized the high-performance computational capabilities of the Biowulf Linux cluster at the National Institutes of Health, Bethesda, MD (http://biowulf.nih.gov).

References

1. Rose G.D., Gierasch L.M., Smith J.A. (1985) Turns in peptides and proteins. Adv Protein Chem;37:1–109.
2. Marshall G.R. (1992) Three-dimensional structure of peptide-protein complexes: implications for recognition. Curr Opin Struct Biol;2:904–919.

3. Marshall G.R. (2001) Peptide interactions with G-protein coupled receptors. Biopolymers;60:246–277.
4. Tyndall J.D.A., Pfeiffer B., Abbenante G., Fairlie D.P. (2005) Over one hundred peptide-activated G protein-coupled receptors recognize ligands with turn structure. Chem Rev;105:793–826.
5. Marshall G.R. (1993) A hierarchical approach to peptidomimetic design. Tetrahedron;49:3547–3558.
6. Che Y. (2003) Protein-protein Recognition: Structure, Energetics and Drug Design. PhD thesis, Washington University, St Louis, Missouri.
7. Che Y., Brooks B.R., Marshall G.R. (2006) Development of small molecules designed to modulate protein-protein interactions. J Comput Aided Mol Des;20:109–130.
8. Pfaff M., Tangemann K., Muller B., Gurrath M., Muller G., Kessler H., Timpl R., Engel J. (1994) Selective recognition of cyclic RGD peptides of NMR defined conformation by αIIbβ3, αVβ3, and α5β1 integrins. J Biol Chem;269:20233–20238.
9. Haubner R., Finsinger D., Kessler H. (1997) Stereoisomeric peptide libraries and peptidomimetics for designing selective inhibitors of the $\alpha_V\beta_3$ integrin for a new cancer therapy. Angew Chem Int Ed Engl;36:1375–1389.
10. Nikiforovich G.V., Kover K.E., Zhang W.J., Marshall G.R. (2000) Cyclopentapeptides as flexible conformational templates. J Am Chem Soc;122:3262–3273.
11. Marshall G.R. (2001) From Merrifield to MetaPhore: a random walk with serendipity. Proceedings of 17th American Peptide Symposium. In: Peptides: the wave of the future. Houghten R.A., Lebl M., editors. San Diego, California: American Peptide Society;p. 3–11.
12. Reaka A.J., Ho C.M., Marshall G.R. (2002) Metal complexes of chiral pentaazacrowns as conformational templates for beta-turn recognition. J Comput Aided Mol Des;16:585–600.
13. Aston K.W., Henke S.L., Modak A.S., Riley D.P., Sample K.R., Weiss R.H., Neumann W.L. (1994) Asymmetric-synthesis of highly functionalized polyazamacrocycles via reduction of cyclic peptide precursors. Tetrahedron Lett;35:3687–3690.
14. Zhang W.-J., Wu Y., Gao Y., Poreddy A.R., Slomczynska U., Chang L., Weber M.E., Marshall G.R. (2003) Metal-pentaazacrown pepridomimetics: RGD and WRY. Proceedings of the 18th American Peptide Symposium. In: Peptide revolution: genomics, proteomics & therapeutics. Chorev M., Sawyer, T.K., editors. Boston, Massachusetts: p. 196–197.
15. Xiong J.P., Stehle T., Zhang R.G., Joachimiak A., Frech M., Goodman S.L., Aranout M.A. (2002) Crystal structure of the extracellular segment of integrin $\alpha_V\beta_3$ in complex with an Arg-Gly-Asp ligand. Science;296:151–155.
16. Etzkorn F.A., Guo T., Lipton M.A., Goldberg S.D., Bartlett P.A. (1994) Cyclic hexapeptides and chimeric peptides as mimics of tendamistat. J Am Chem Soc;116:10412–10425.
17. Matter H., Kessler H. (1995) Structures, dynamics, and biological-activities of 15 cyclic hexapeptide analogs of the α-amylase inhibitor tendamistat (Hoe-467) in solution. J Am Chem Soc;117:3347–3359.
18. Riley D.P., Weiss R.H. (1994) Manganese macrocyclic ligand complexes as mimics of superoxide-dismutase. J Am Chem Soc;116:387–388.
19. Riley D.P., Henke S.L., Lennon P.J., Weiss R.H., Neumann W.L., Rivers W.J., Aston K.W., Sample K.R., Rahman H., Ling C.S., Shieh J.J., Busch D.H., Szulbinski W. (1996) Synthesis, characterization, and stability of manganese(II) C-substituted 1,4,7,10,13-pentaazacyclopentadecane complexes exhibiting superoxide dismutase activity. Inorg Chem;35:5213–5231.
20. Riley D.P., Lennon P.J., Neumann W.L., Weiss R.H. (1997) Toward the rational design of superoxide dismutase mimics: mechanistic studies for the elucidation of substituent effects on the catalytic activity of macrocyclic manganese(II) complexes. J Am Chem Soc;119:6522–6528.
21. Salvemini D., Wang Z.Q., Zweier J.L., Samouilov A., Macarthur H., Misko T.P., Currie M.G., Cuzzocrea S., Sikorski J.A., Riley D.P. (1999) A nonpeptidyl mimic of superoxide dismutase with therapeutic activity in rats. Science;286:304–306.
22. Riley D.P., Henke S.L., Lennon P.J., Aston K. (1999) Computer-aided design (CAD) of synzymes: use of molecular mechanics (MM) for the rational design of superoxide dismutase mimics. Inorg Chem;38:1908–1917.
23. Riley D.P. (1999) Functional mimics of superoxide dismutase enzymes as therapeutic agents. Chem Rev;99:2573–2587.
24. Aston K., Rath N., Naik A., Slomczynska U., Schall O.F., Riley D.P. (2001) Computer-aided design (CAD) of Mn(II) complexes: superoxide dismutase mimetics with catalytic activity exceeding the native enzyme. Inorg Chem;40:1779–1789.
25. Salvemini D., Riley D.P., Cuzzocrea S. (2002) SOD mimetics are coming of age. Nat Rev Drug Discov;1:367–374.
26. Macarthur H., Westfall T.C., Riley D.P., Misko T.P., Salvemini D. (2000) Inactivation of catecholamines by superoxide gives new insights on the pathogenesis of septic shock. Proc Natl Acad Sci U S A;97:9753–9758.
27. Samlowski W.E., Petersen R., Cuzzocrea S., Macarthur H., Burton D., McGregor J.R., Salvemini D. (2003) A nonpeptidyl mimic of superoxide dismutase, M40403, inhibits dose-limiting hypotension associated with interleukin-2 and increases its antitumor effects. Nat Med;9:750–755.
28. Aquaro S., Muscoli C., Pollicita M., Ranazzi A., Granato T., Bellocchi M.C., Modesti A., Salvemini D., Mollace V., Perno C.F. (2005) Selective removal of superoxide anions is crucial for HIV replication in human primary macrophages and prevents peroxynitrite mediated apoptosis in neurons. Antiviral Res;65:A28–A28.
29. Schafer A., Horn H., Ahlrichs R. (1992) Fully optimized contracted gaussian-basis sets for atoms Li to Kr. J Chem Phys;97:2571–2577.
30. Schafer A., Huber C., Ahlrichs R. (1994) Fully optimized contracted gaussian-basis sets of triple zeta valence quality for atoms Li to Kr. J Chem Phys;100:5829–5835.
31. Che Y., Marshall G.R. (2006) Engineering cyclic tetrapeptides containing chimeric amino acids as preferred reverse-turn scaffolds. J Med Chem;49:111–124.
32. Shannon R.D. (1976) Revised effective ionic-radii and systematic studies of interatomic distances in halides and chalcogenides. Acta Crystallogr A;32:751–767.